Electrochimica Acta 215 (2016) 435–446

Contents lists available at ScienceDirect

Electrochimica Acta

journal homepage: www.elsevier.com/locate/electacta

Preparation of $SrTiO_3$ perovskite decorated rGO and electrochemical detection of nitroaromatics

Khursheed Ahmad[a], Akbar Mohammad[a], Pradeep Mathur[a,*], Shaikh M. Mobin[a,b,c,*]

[a] Discipline of Chemistry, Indian Institute of Technology Indore, Simrol, Indore 453552, India
[b] Metallurgical Engineering and Material Science, Indian Institute of Technology Indore, Simrol, Indore 453552, India
[c] Centre for Biosciences and Bio-Medical Engineering, Indian Institute of Technology Indore, Simrol, Indore 453552, India

ARTICLE INFO

Article history:
Received 30 June 2016
Received in revised form 20 August 2016
Accepted 26 August 2016
Available online 27 August 2016

Keywords:
Perovskite
rGO-SrTiO3 nanocomposite
Explosives sensing
Cyclic voltammetry
Differential pulse voltammetry

ABSTRACT

A perovskite ($SrTiO_3$) and reduced graphene oxide (rGO) based nanocomposite (rGO/$SrTiO_3$) material has been synthesized *in*-situ. The rGO/$SrTiO_3$ nanocomposite was characterized by PXRD, SEM, EDX mapping, TEM and SAED pattern to confirm its purity and morphology. The surface of the glassy carbon electrode (GCE) was modified by coating rGO/$SrTiO_3$ nanocomposite without any binder. This modified electrode GCE-rGO/$SrTiO_3$ (**MGCE**) was employed for electrochemical detection of nitro-substituted aromatics such as *p*-nitrophenol (*p*-NP), 2,4-dinitrophenol (2,4-DNP), 2,4-dinitrotoluene (2,4-DNT) and 2,4,6-trinitrophenol (TNP) which shows a rapid electronic communications. The **MGCE** exhibited the limit of detection (LOD) of 110 nM, 134 nM, 128 nM, 146 nM, high sensitivity of 193.43 $\mu A\,\mu M^{-1}\,cm^{-2}$, 25.34 $\mu A\,\mu M^{-1}\,cm^{-2}$, 71.66 $\mu A\,\mu M^{-1}\,cm^{-2}$, 13.16 $\mu A\,\mu M^{-1}\,cm^{-2}$ and a linear range between 0.3–0.8, 0.4–0.7, 0.5–0.8, 0.5–0.7 μM for *p*-NP, 2,4-DNP, 2,4-DNT and TNP, respectively. The developed MGCE sensor thus implemented is also advantageous for its low cost, stability, reliability and rendering applications for real system analysis.

© 2016 Published by Elsevier Ltd.

1. Introduction

In general, ABO_3 type metal oxides are the most stable perovskite which exhibits peculiar and fascinating properties such as superconductivity, ferroelectricity, charge ordering, ferromagnetism, and magnetism [1]. The perovskite has been employed in various fields such as solar cells [2], photo degradation of dyes [3], semiconductor based electrical devices, Li-ion batteries [4], supercapacitors [5] and also in fabrication of gas [6–8] and electrochemical sensors [9] because of their excellent properties. $SrTiO_3$ considered being a novel material that can be used in the fabrication of binder free highly sensitive electrochemical sensor. On the other hand, reduced graphene oxide (rGO) exhibits outstanding properties such as high electrical and thermal conductivity, electron mobility, chemical stability and higher mechanical strength which makes it an ideal candidate to integrate to form a highly functional composite with other nanomaterial's and metal oxides which accelerate the performances [10–13].

A derivative of phenol family such as *p*-nitrophenol (*p*-NP) is a product or intermediate which produced during the degradation of pesticides like organo-phosphorus. Therefore, a highly reliable, efficient, highly sensitive and robust chemical sensor is desired for the detection of *p*-NP and their derivatives. The detection of nitroaromatics (TNP, DNT, TNT etc.) have grown security and environmental concerns due to threat of terrorist activities and their hazards, have generated major demand for innovative, field-deployable tools for detecting explosives in a fast, sensitive, reliable and simple manner [14]. Conventional methods like gas chromatography [15,16], fluorescence [17], capillary electrophoresis [18], high performance liquid chromatography [19], ion mobility spectrometry (IMS) and liquid chromatography along with mass spectrometry and others have been widely used for the detection of hazardous and explosive chemicals [20]. These techniques are costly and difficult to handle and require long time for analysis. The electrochemical sensors possess many advantages for use in detection of explosives, including high sensitivity and selectivity, speed, wide linear range, minimal space and power requirements, and low-cost instrumentation. These factors render electrochemical detection of explosives very attractive, and within the scope of a variety of laboratories and industry based detection applications [21].

* Corresponding authors at: Discipline of Chemistry, Indian Institute of Technology Indore, Simrol, Indore 453552, India.
E-mail address: xray@iiti.ac.in (S.M. Mobin).

http://dx.doi.org/10.1016/j.electacta.2016.08.123
0013-4686/© 2016 Published by Elsevier Ltd.

Although there are few reports on the detection of *p*-NP based on CuO nanotubes [22], MnO_2 [23], ZnOnanoflower [24], rGO/Au nanocomposite [25], Mg(Ni)FeOnanocomposite [26] and metal oxide-composite nanoparticles by employing electrochemical method. There are also reports on the detection of 2,4-DNT and TNP using various modified electrodes such as screen printed electrode, N-doped rGO/CuS composite, functionalized and electrochemically rGO and sonogel carbon [27–31]. Further, the sensing of 2,4-DNP, 2,4-DNT and TNP remains a challenging task and needs immediate attention by developing a highly selective and sensitive sensor [32].

So far, most of the results related to the detection of explosives have the following disadvantages: (i) use of expensive metal such as Au, Pt, Ag and Ru based composites [20,21], (ii) lack of distinct identification of each NO_2 group present in the explosives (2,4-DNP, 2,4-DNT, and TNP) [29], (iii) required appropriate binder and (iv) lack of sensitivity and selectivity. To overcome such issues we introduce a binder free $SrTiO_3$ perovskite based modified electrode which is less expensive, highly sensitive and selective with distinct identification of each NO_2 group present in the nitroaromatics (*p*-NP, 2,4-DNP, 2,4-DNT and TNP).

To the best of our knowledge, so far no report available on rGO/$SrTiO_3$nanocomposite as modified glassy carbon electrode (**MGCE**) based *p*-NP sensor. In this work, we demonstrate use of the **MGCE** for the sensing of *p*-NP as well as other nitro group containing explosive compounds such as 2,4-DNP, 2,4-DNT and TNP which shows excellent results. The rGO sheets overlap with $SrTiO_3$ provide (i) the complex conducting network for fast electron transfer between the active materials and the charge collectors and (ii) improves the contact between the electrode material and the electrolyte. Therefore, the combination of rGO with $SrTiO_3$ was found to be an efficient object to promote the electron for the electrochemical detection of nitro aromatics.

2. Materials and Methods

2.1. Cautions

The studied nitroaromatics {*p*-nitrophenol (*p*-NP), 2,4-dinitrophenol (2,4-DNP), 2,4-dinitrotoluene (2,4-DNT) and 2,4,6-trinitrophenol (TNP)} are highly toxic/explosives. The solutions for the study should prepare in very low concentration and handled with great care with proper precautions. For more details on handling MSDS sheet should be followed.

2.2. Chemicals and reagents

All the chemicals were purchased from Sigma Aldrich and Alfa Aesar were used as received.

2.3. Instrumentation

The powder x-ray diffraction patterns (PXRD) were recorded on a Rigaku, Japan, RINT 2500 V x-ray diffractometer with Cu Kα irradiation (λ = 1.5406 Å). The morphologies and elemental constituents of the samples were characterized using Supra 55 Zeiss Field Emission Scanning Electron microscope (FESEM) attached with Energy Dispersive X-ray (EDX) spectroscopy (Oxford Instrument' X-max, AZtec). Further, more information about the morphological characteristics and size was examined by Transmission Electron Microscopy (TEM) using FEI Tecnai G2 12 Twin TEM 120 kV. All electrochemical measurements were performed on Metrohm Autolab PGSTAT 302N using NOVA software version 1.10. The GCE as a working electrode, platinum wire as a counter electrode and Ag/AgCl as a reference electrode were used for all electrochemical measurements.

2.4. Synthesis of graphene oxide (GO) and reduced graphene oxide (rGO)

GO was synthesized according to the well-known Hummer's method with some modifications [33]. In a typical synthesis of GO, 1.0 g of graphite flakes and 0.5 g of $NaNO_3$ was stirred simultaneously in concentrated H_2SO_4 (23.0 mL) and stirred for 30 min at room temperature. Further, 3.0 g of $KMnO_4$ was added slowly on ice bath to maintain the temperature below 20 °C to avoid the large exotherm and stirred continuously overnight at 35 °C. Subsequently, D.I. water (60.0 mL) was added to the reaction mixture. Additionally, 1.5 g of $KMnO_4$ was also added gradually and the reaction was further continued at 35 °C for 14 h. The mixture was kept at room temperature to cool down and 500 mL of D.I. water was added with 30% of H_2O_2 (7.0 mL). The obtained suspension was further washed with D.I. water to separate the solid product and unreacted materials. The product was further washed with 1 M HCl solution repeatedly. The final product was washed with excess D.I. water and dried under vacuum at 50 °C for 6 h to get the desired product. The obtained GO was chemically reduced to rGO using hydrazine hydrate as reported elsewhere [34].

2.5. Synthesis of $SrTiO_3$

The $SrTiO_3$ was synthesized by solvothermal method. In a typical synthesis of $SrTiO_3$, 25.0 mL diethylene glycol, (DEG) and 0.13 M $Sr(OH)_2.8H_2O$ were added into the 50 ml of round bottom flask (r.b. flask) and heated to 60 °C for 3 h at stirring condition to make the solution homogenous. To the above reaction mixture, 0.18 M of $Ti(OBu)_4$ was added under stirring followed by addition of tetra butyl ammonium hydroxide (TBAH, 4.0 mL) to the above reaction mixture. Further, the reaction was continued for 2 h at 60 °C and final reaction mixture was transferred to the Teflon lined stainless steel autoclave and kept at furnace operated at180 °C for 24 h. After cooling to room temperature (RT), the obtained $SrTiO_3$ nanoparticles were washed repeatedly with ethanol and water and dried in the oven at 70 °C.

2.6. Synthesis of rGO/$SrTiO_3$ nanocomposite

Insitu synthesis of rGO/$SrTiO_3$ nanocomposite was carried out using solvothermal method (Scheme 1). For the synthesis of rGO/$SrTiO_3$, 25.0 mL diethylene glycol, (DEG) and 0.13 M Sr $(OH)_2.8H_2O$ were added into the 50 ml of r.b. flask at 60 °C for 3 h at stirring condition to make the solution homogenous. To this, GO (45.0 mg) was added to the above homogenized solution and subsequently it was ultrasonicated for approximately 1 h to disperse the GO. Further, 0.18 M of $Ti(OBu)_4$ was added under stirring followed by addition of TBAH (4.0 mL) to the above reaction mixture and the reaction was continued for 2 h at 60 °C. Finally, the solution was transferred to the Teflon lined stainless steel autoclave vessel and kept at furnace operated at180 °C for 24 h. After cooling to room temperature (RT), the obtained rGO/$SrTiO_3$ nanocomposite were washed repeatedly with ethanol and water and dried in the oven at 70 °C.

2.7. Fabrication of MGCE Sensor

The nanoparticles composite (rGO/$SrTiO_3$) has been employed to fabricate the sensor by the dispersion of nanocomposite in D.I. water and drop casted onto the surface of glassy carbon electrode (GCE) and allowed to dry for 3 h (GCE was cleaned using alumina slurry and sonicated for 20 min before the fabrication of the sensor). Further, this MGCE was employed to detect the nitroaromatics (*p*-NP, 2,4-DNP, 2,4-DNT and TNP).

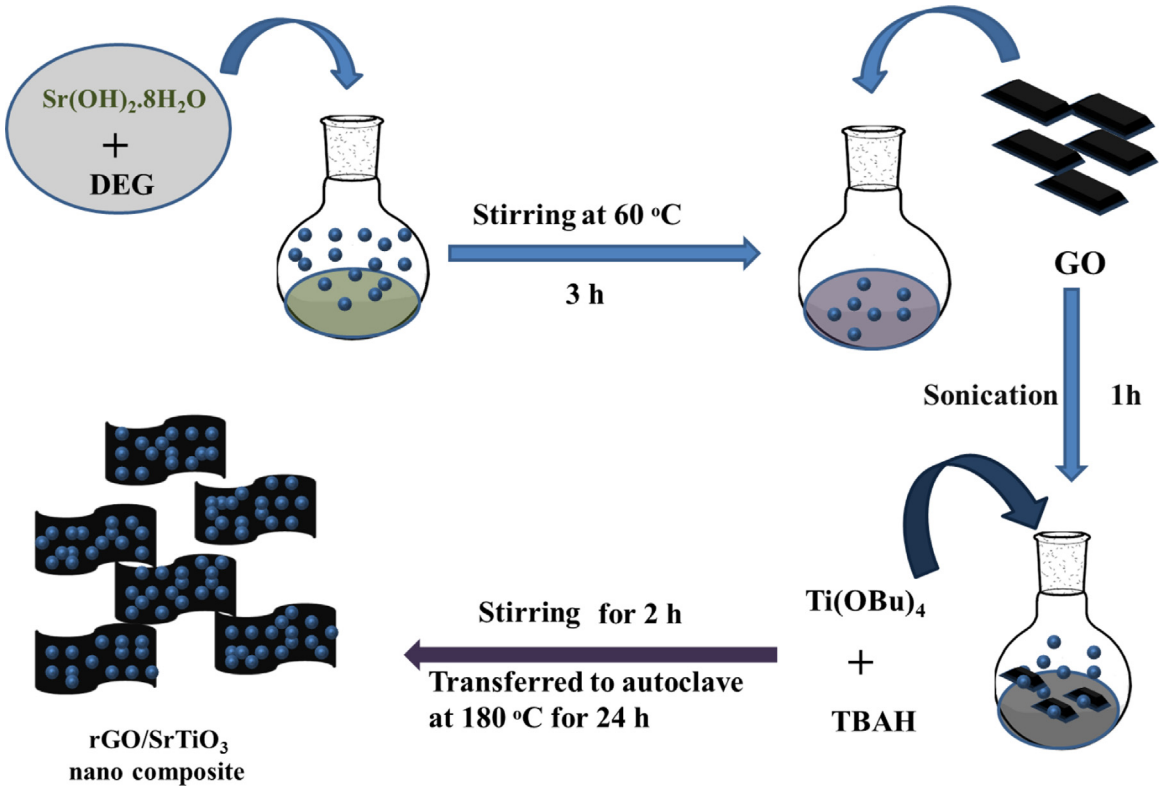

Scheme 1. Schematic representation for *insitu* grown **rGO/$SrTiO_3$**.

3. Results and discussion

3.1. Insitu *synthesis of $SrTiO_3$ perovskite decorated rGO*

Insitu $SrTiO_3$ perovskite decorated rGO nanocomposite (rGO/$SrTiO_3$) has been synthesized using solvothermal approach as shown in Scheme 1. *Insitu* grown rGO/$SrTiO_3$ nanocomposite was further characterized by PXRD, FESEM, EDX and TEM.

3.2. *Characterization of rGO/$SrTiO_3$ nanocomposite*

The XRD pattern for GO shows the presence of a broad peak (10.8) which corresponds to GO (Fig. 1a). The peaks for rGO/$SrTiO_3$ was in agreement with previously reported literature as shown in Fig. 1(b).[29] The peaks present at 25.4° and 36.4° were corresponds to existence of TiO_2. However, due to the presence of low amount of rGO, the peak for the rGO could not appear in the XRD patterns. For comparison, rGO and $SrTiO_3$ were separately synthesized and the XRD patterns for the rGO and $SrTiO_3$ were shown in Figs. (S1and S1). The peak at 10.8° was disappeared and a new broad peak was observed at 25.6° corresponding to the rGO which shows the reduction of GO to the rGO. The XRD peaks for the $SrTiO_3$ matches well with the reported literature with presence of TiO_2 as the mixed phase due to less time of the synthesis as compare to previous reports [35,36].

The morphological features of GO, $SrTiO_3$ and rGO/$SrTiO_3$ were analyzed by the scanning electron microscopy (SEM). The SEM image shows the GO sheets (Fig. S3) and the $SrTiO_3$ spherical nanoparticles with nearly10 nm in diameter (Fig. 2a and b). Moreover, rGO/$SrTiO_3$ nanocomposite shows that $SrTiO_3$ nanoparticles were adhered to the rGO sheet as shown in Fig. 2(c and d). This strong binding of $SrTiO_3$ nanoparticles on graphene sheets results in a smooth pathway for electron transportation and collection. Additionally, EDX mapping has been performed which shows presence of Sr, Ti, O and C thus confirmed formation of rGO/$SrTiO_3$ nanocomposites (Figs. 3 and 4).

Transmission electron microscopy (TEM) and high magnification transmission electron microscopy images of the rGO/$SrTiO_3$ nanocomposite were shown in Fig. 5(a–c). Similar to SEM, $SrTiO_3$ nanoparticles were found to be in spherical form and with the diameter in the range of 10–30 nm which were decorated on graphene sheet. The regular crystal diffraction spots present in SAED pattern of rGO/$SrTiO_3$ nanocomposite shown in the inset of

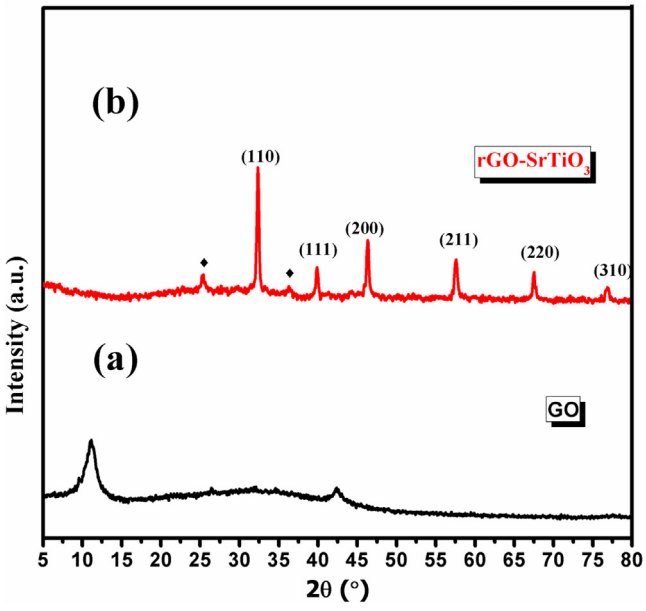

Fig. 1. XRD pattern of GO and rGO/$SrTiO_3$.

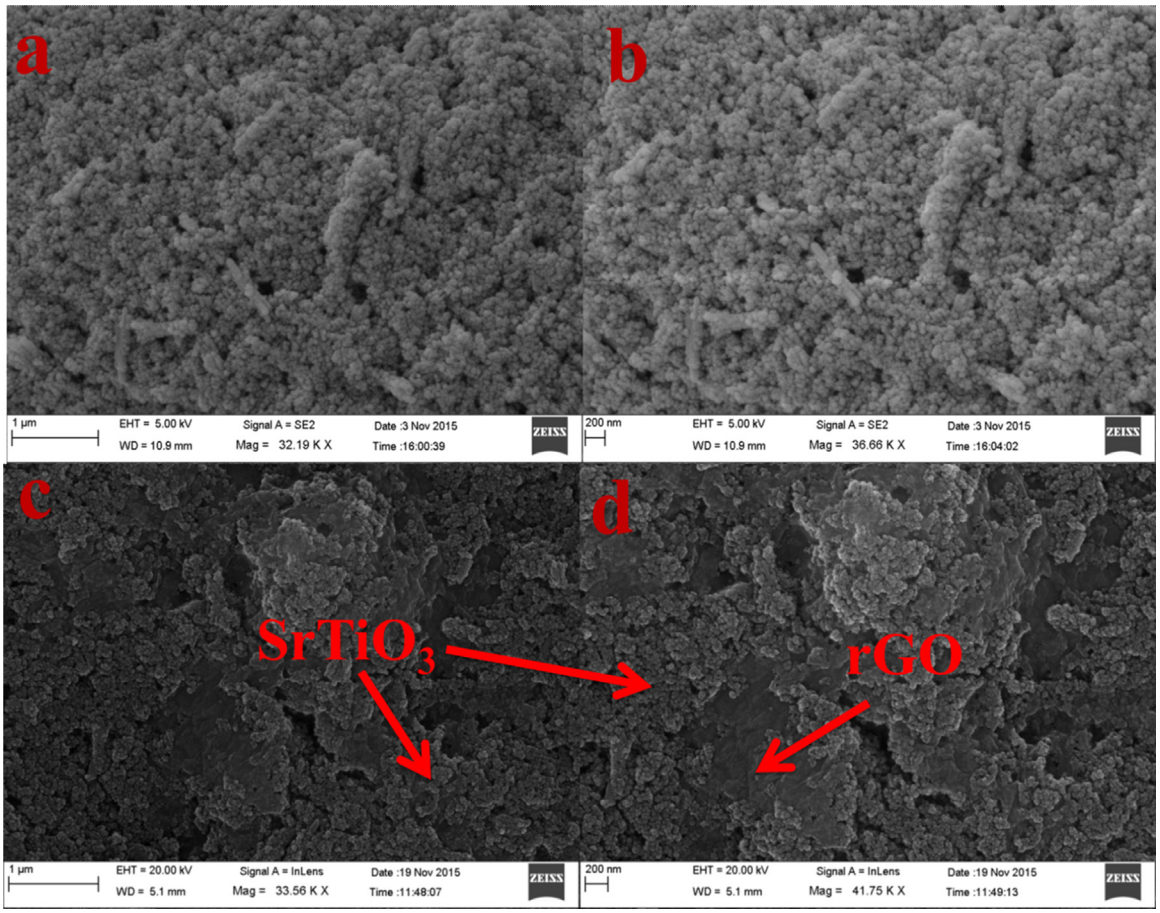

Fig. 2. FE-SEM image of $SrTiO_3$ nanoparticles (a and b) and rGO/$SrTiO_3$ nanocomposite (c and d) at different magnifications.

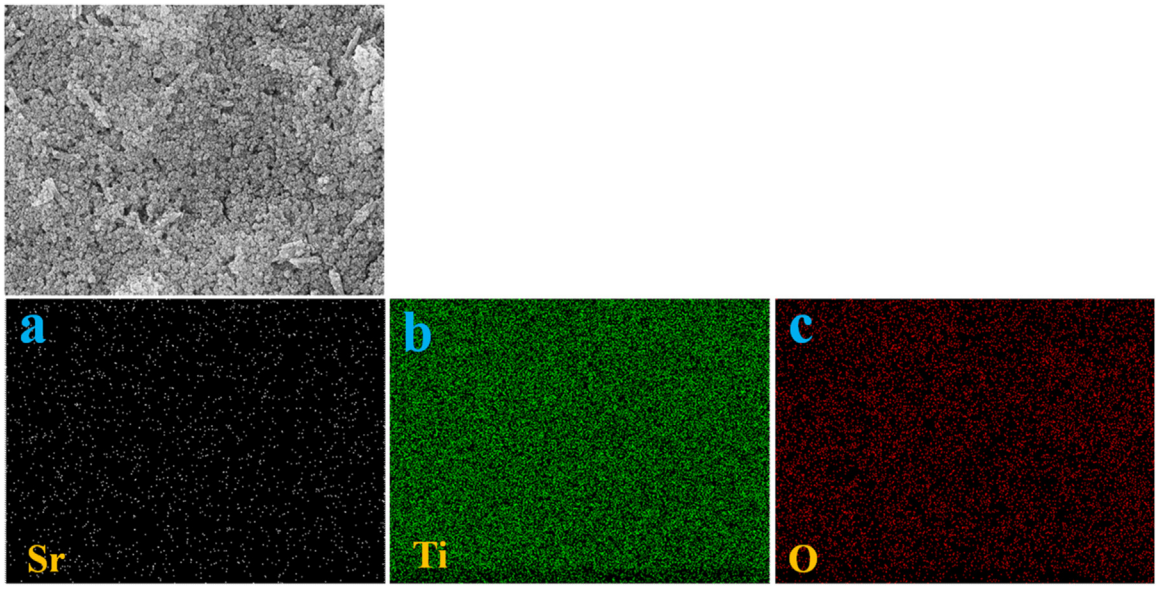

Fig. 3. EDS mapping of $SrTiO_3$.

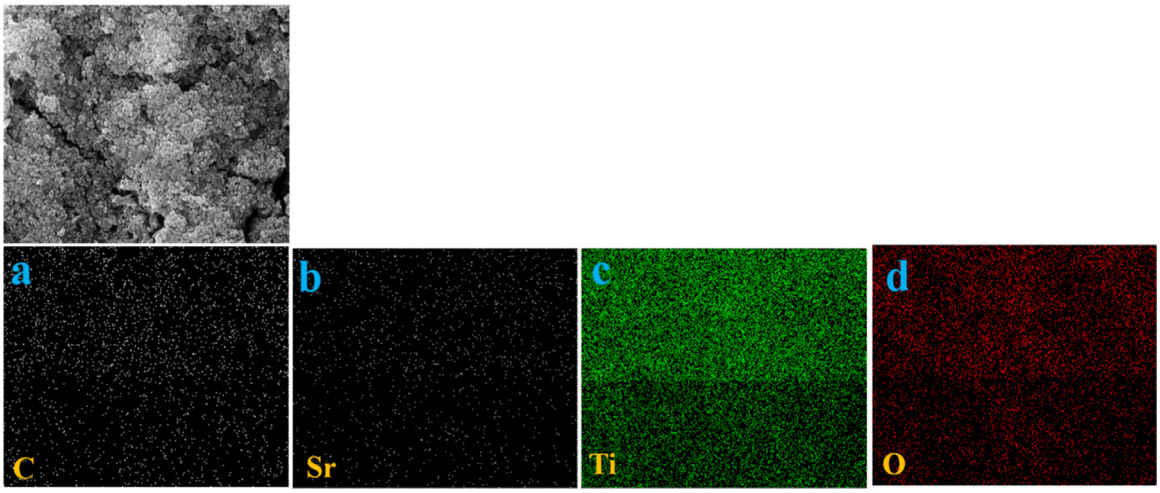

Fig. 4. EDS mapping of rGO/$SrTiO_3$.

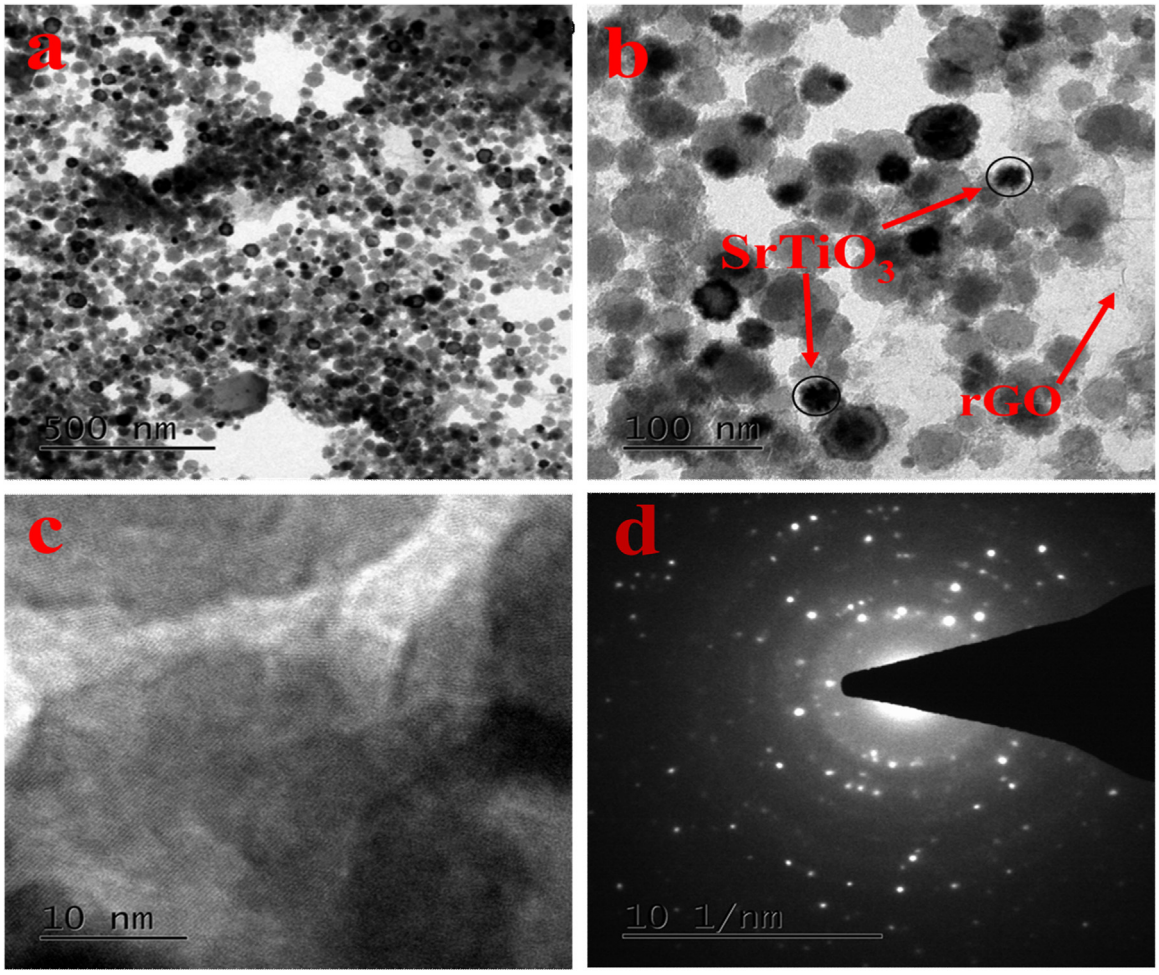

Fig. 5. TEM of rGO/$SrTiO_3$.

Fig. 5(d) indicates that synthesized composites have crystalline nature of the particles.

3.3. Electrochemical impedance spectroscopy (EIS) study

The charge transfer behavior at different modified GCE surfaces has been investigated using impedance study. The Nyquist plot for the four different modified electrodes a) Bare, b) $SrTiO_3$, c) rGO and d) rGO/$SrTiO_3$ with a frequency range from 0.01 Hz to 100 kHz in PBS of pH 7.0 are shown in Fig. 6, in which the imaginary impedance (-Z″) was plotted against the real impedance (Z′). The bare GCE, $SrTiO_3$ and rGO exhibited very high charge resistance whereas a lower resistance was obtained for **MGCE** which suggested the better electron transfer as compared to the bare

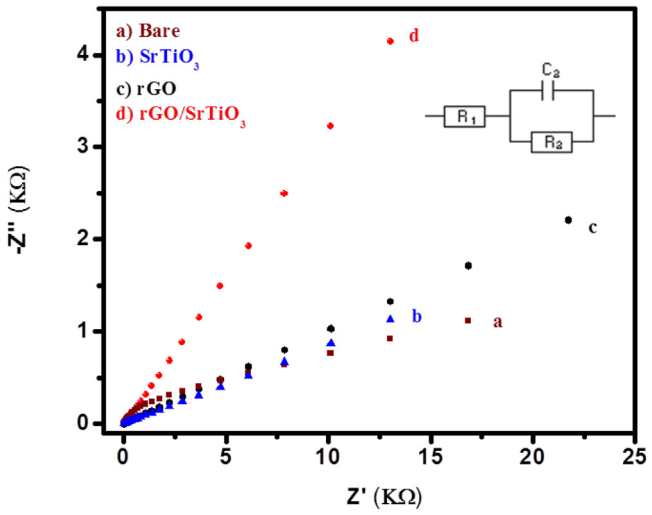

Fig. 6. Nyquist plot of (a) GCE, (b) $SrTiO_3$, (c) rGO and (d) rGO/$SrTiO_3$ in PBS (pH 7.0).

GCE and other modified electrodes. It is to be noted that the higher charge resistance (Rct) limits the electron transfer mechanism. The equivalent circuit was obtained by fitting the EIS data and inserted in inset of Fig. 6, and charge resistance was summarized in Table (S1).

3.4. Electrochemical performance of the rGO/$SrTiO_3$ nanocomposite (MGCE) based nitro sensor

Fig. 7 shows the cyclic voltammograms (CVs) of bare (a) and **MGCE** (b) in PBS at pH 7.0 resulting enhanced current for **MGCE** as compared to bare electrode After evaluation of bare and **MGCE** performances, further the response of **MGCE** was examined on different nitroaromatics such as *p*-NP, 2,4-DNP, 2,4-DNT and TNP. Fig. 8(A) shows the CVs of the bare and **MGCE** in the presence of *p*-NP and an improved current with new oxidation and reduction peaks of the *p*-NP was obtained for **MGCE.**

In presence of *p*-NP the CVs shows distinctly an irreversible reduction peak (R1) at −0.71 V and a pair of new reversible reduction and oxidation peaks at 0.04 V and 0.15 V, respectively, at **MGCE**. It is to be noted that with increase in the number of nitro group in the aromatic ring, this increases the explosiveness nature

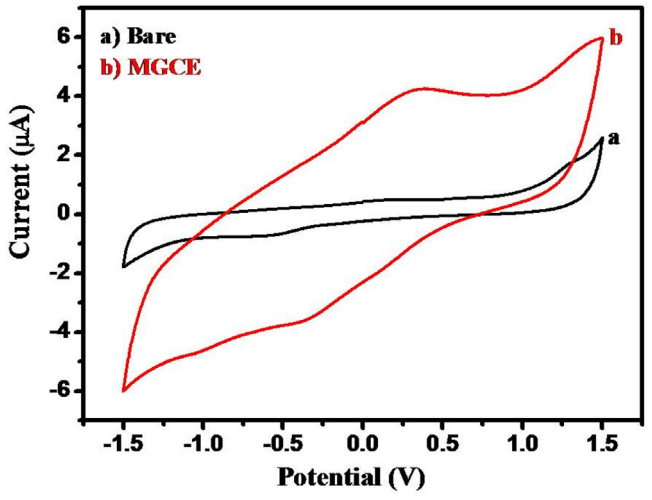

Fig. 7. Cyclic voltammograms of (a) bare and (b) **MGCE** in PBS (pH 7.0) with a scan potential of 100 mV/s.

of nitro compounds. Therefore, the cyclic voltammetry measurements was further extended towards 2,4-DNP, 2,4-DNT and TNP as shown in Fig. 8(B–D respectively). Fig. 8(A–D) demonstrate that the highest current for **MGCE** were obtained for all the four nitro aromatics as compare to bare electrode. To explore the effect of $SrTiO_3$ and rGO as modified electrode, we have compared GCE/$SrTiO_3$ and GCE/rGO electrodes in PBS (pH 7.0) and found that GCE/rGO modified electrode shows higher current compared to the GCE/$SrTiO_3$ modified electrode but the current obtained for both these electrodes were less as compared to the **MGCE** shown in Fig. (S4). Further, GCE/$SrTiO_3$ and GCE/rGO modified electrodes were also investigated in the presence of *p*-NP, 2,4-DNP, 2,4-DNT and TNP. The lower current values were obtained for GCE/rGO and GCE/$SrTiO_3$ and the relatively higher current was obtained for **MGCE** (Figs. S5–S8).

Further, the differential pulse voltammetry (DPV) was employed for four nitroaromatics which also revealed that highest current was obtained for **MGCE** as compared to bare GCE Fig. 9(A–D).

The effect of various concentrations from 0.1 to 1 μM in PBS at pH 7.0 was performed by employing cyclic voltammetry towards **MGCE** against *p*-NP, 2,4-DNP, 2,4-DNT and TNP (Fig. 10). The results obtained from this revealed that with increase in the concentration of the *p*-NP the irreversible reduction peak (O_1) also increases which suggested that **MGCE** shows sensitive and fast response towards *p*-NP. This good electrical response of the **MGCE** may be due to the redox reaction and good electrocatalytic properties of the rGO/$SrTiO_3$ nanoparticles composite. A typical linear relation graph for the anodic current peaks against the different concentration of *p*-NP was plotted in inset of Fig. 10(A). Similarly, the response current for 2,4-DNP, 2,4-DNT and TNP also increases linearly and their calibration plots of the current peaks against the concentrations have been inserted in the inset of Fig. 10(B–D).

The effect of scan rate on the cyclic voltammetry of *p*-NP, 2,4-DNP, 2,4-DNT and TNP were also investigated and depicted in Fig. 11(A–D). The electrocatalytic current for all nitroaromatics increases with the increase in the scan rate from 100–1000 mV/s. The calibration plots of current peak against the square root of the scan rate are plotted in the inset of Fig. 11(A–D).

Further, to endorse the results obtained by CV and DPV we have employed linear sweep voltammetry for *p*-NP, 2,4-DNP, 2,4-DNT and TNP against **MGCE.** Fig. 12(A–D) shows that with increasing in the concentration of the *p*-NP, 2,4-DNP, 2,4-DNT and TNP the current peak was also increased. A calibration curve of the current peak against the concentration of the *p*-NP, 2,4-DNP, 2,4-DNT and TNP was plotted and shown in inset of Fig. 12(A–D). Fig. 13(A–D) shows the effect of concentration for all nitroaromatics (*p*-NP, 2,4-DNP, 2,4-DNT and TNP) at different concentrations from 0.1 to 1 μM in PBS at pH 7.0. The electro-catalytic current was increased linearly with increase in the concentration of the nitroaromatics and their calibration plots of the current peaks against the concentrations have been inserted in the inset of Fig. 13(A–D).

The **MGCE** electrode shows excellent results for the detection of *p*-NP, subsequently we also performed the **MGCE** for the detection of 2,4-DNP, TNP and also for explosive 2,4-DNT. In Fig. (S4) we performed the CVs for four different modified electrodes i.e. a) GCE, b) GCE/rGO, c) GCE/$SrTiO_3$ and d) **MGCE** in the presence of 2,4-DNP in PBS of 7.0. The highest electro catalytic current was observed for the **MGCE** electrode among all the four electrodes which revealed that **MGCE** provide an easy way for the electron transfer. Similarly we performed the cyclic voltammetry for the sensing of 2,4-DNP, TNP as shown in Fig. (S5 and S6) and similar results were obtained which prove that **MGCE** efficiently worked for the sensing of nitro aromatics.

The proposed redox reactions takes place during the sensing of the *p*-NP was summarized in Scheme 2.

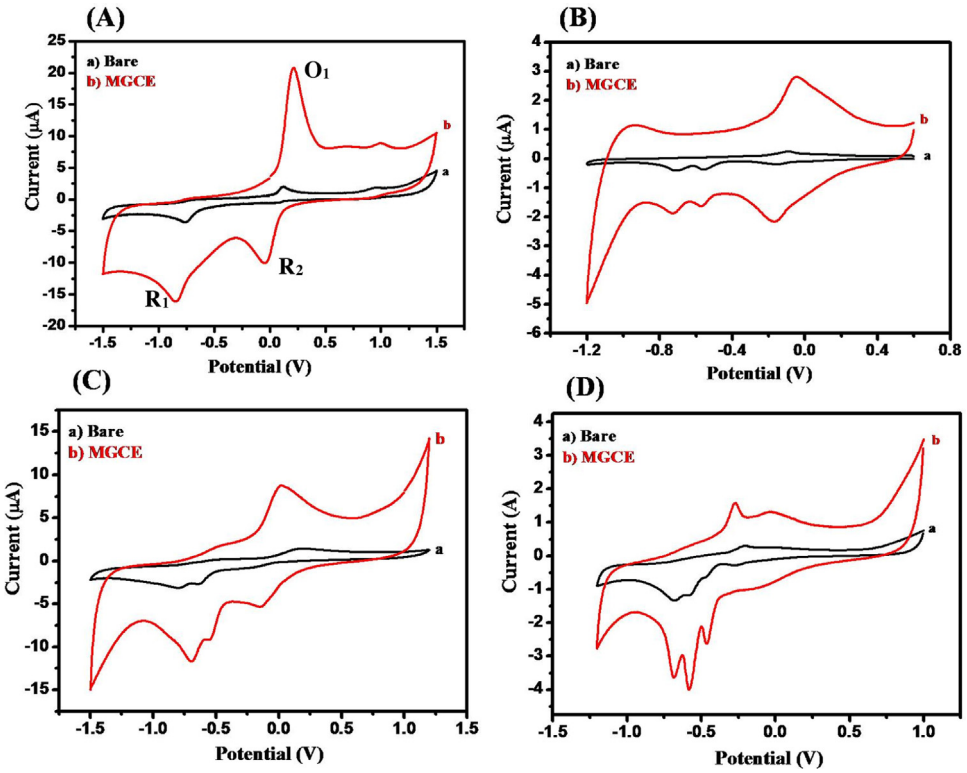

Fig. 8. Cyclic voltammograms (A) for *p*-NP at bare (a) and **MGCE** (b), (B) for 2,4-DNP at bare (a) and **MGCE** (b), (C) for 2,4-DNT at bare (a) and **MGCE** (b) and (D) for TNP at bare (a) and **MGCE** (b) in PBS (pH 7.0) with a scan potential of 100 mV/s.

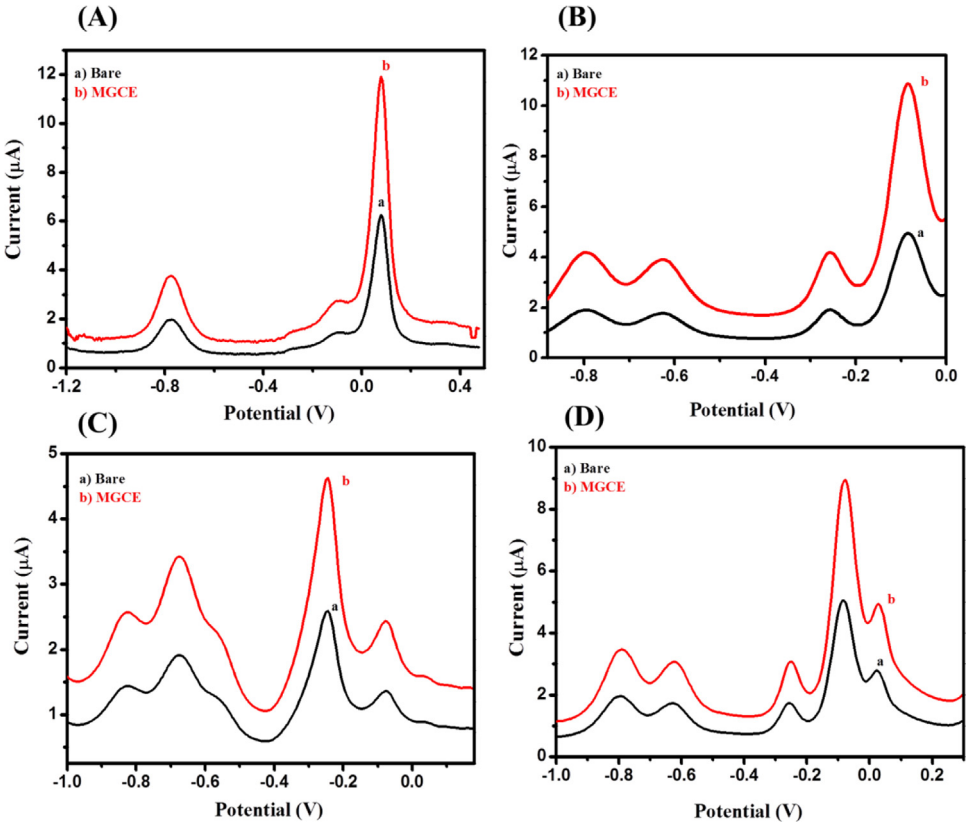

Fig. 9. Differential Pulse voltammograms (A) for *p*-NP at bare (a) and **MGCE** (b), (B) for 2,4-DNP at bare (a) and **MGCE** (b), (C) for 2,4-DNT at bare (a) and **MGCE** (b) and (D) for TNP at bare (a) and **MGCE** (b) in PBS (pH 7.0) with a scan potential of 100 mV/s.

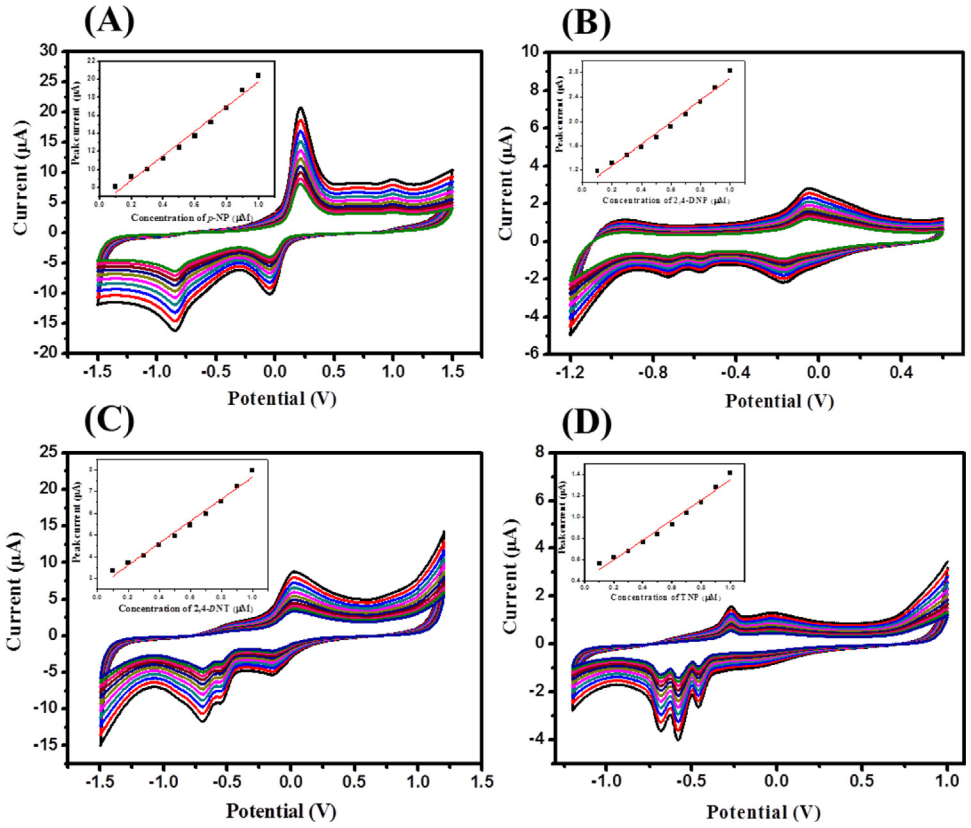

Fig. 10. Cyclic voltammograms of **MGCE** (A) for *p*-NP, (B) for 2,4-DNP, (C) for 2,4-DNT and (D) for TNP at different concentration (0.1–1 μM) in PBS (pH 7.0) with a scan potential of 100 mV/s. The calibration plots of peak current against the concentration are plotted in inset of their corresponding cyclic voltammograms.

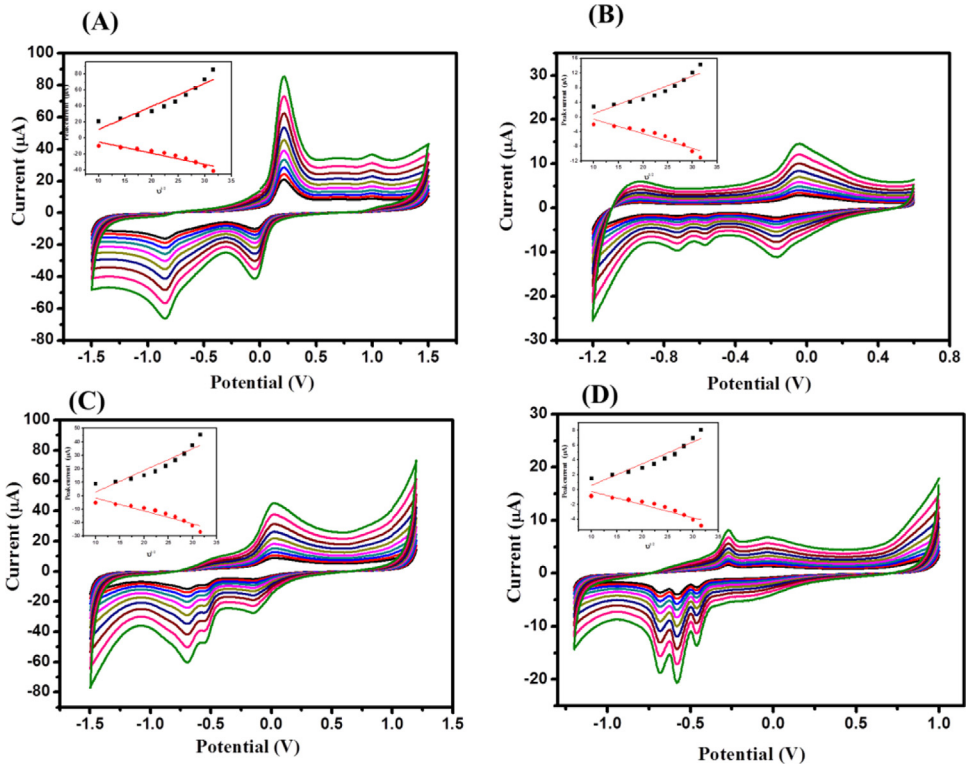

Fig. 11. Cyclic voltammograms of **MGCE** (A) for *p*-NP, (B) for 2,4-DNP, (C) for 2,4-DNT and (D) for TNP in PBS (pH 7.0) at different scan rate (100–1000 mV/s) and inset showing the linear calibration plot against the square root of the scan rate.

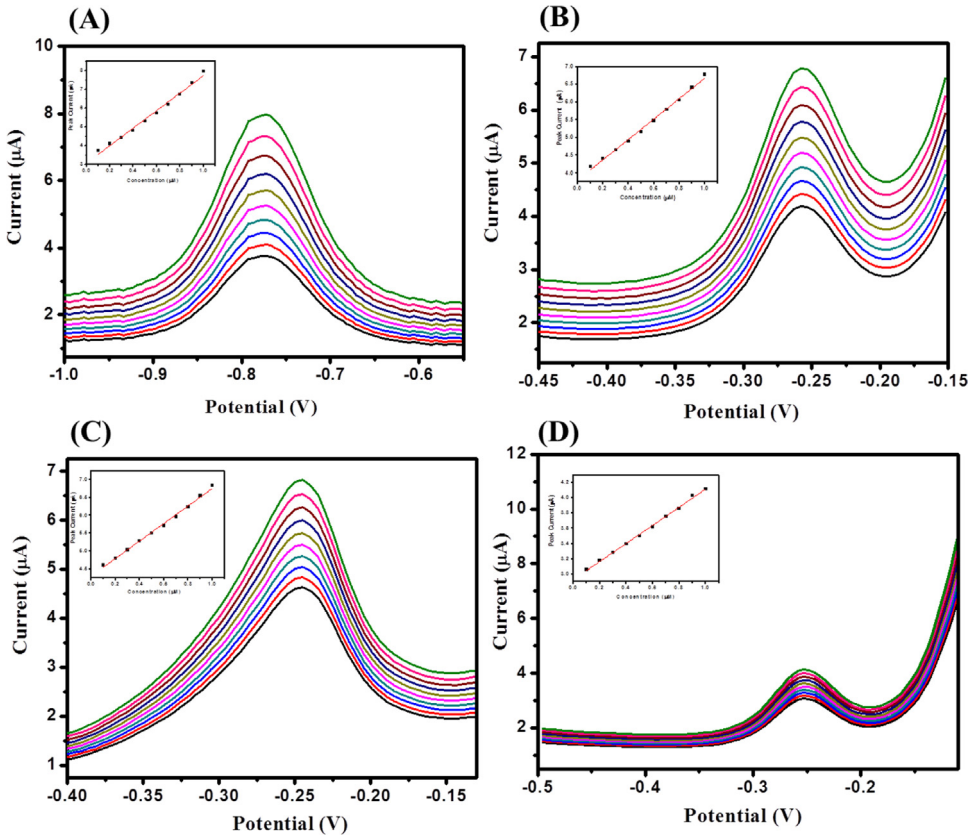

Fig. 12. Differential pulse voltammograms of **MGCE** (A) for *p*-NP, (B) for 2,4-DNP, (C) for 2,4-DNT and (D) for TNP at different concentration (0.1–1 μM) in PBS (pH 7.0) with a scan potential of 100 mV/s. The inset showing the calibration plots of peak current versus concentration.

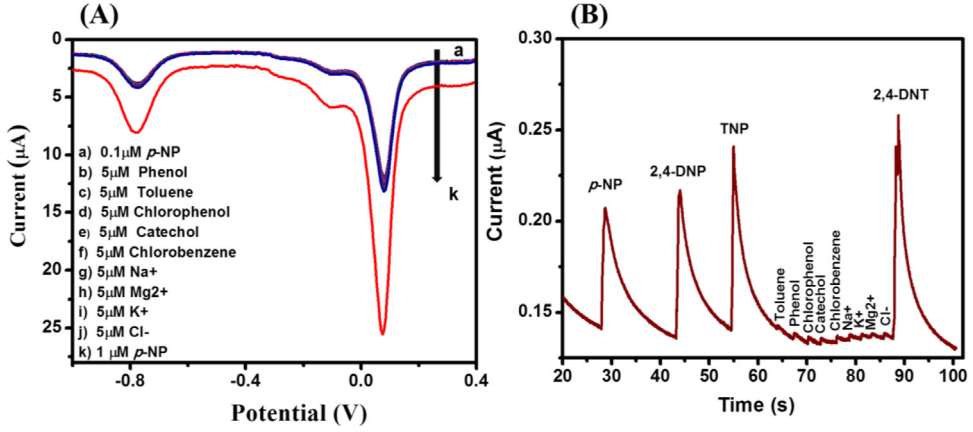

Fig. 13. (A) Interference study for *p*-NP using Differential pulse voltammetry and (B) for nitroaromatics using chronoamperometry in PBS (pH 7.0).

In the proposed mechanism (where, O_1 and R_1, R_2 are denoted for oxidation and reductions, respectively) as shown in Scheme 2. Firstly, a redox reaction occurs and leads to *p*-NP conversion and produces p-hydroxyl-amino-phenol (R1). Secondly, the oxidation of *p*-hydroxyl-amino-phenol proceeds, resulting to *p*-nitroso-phenol and the subsequent reversible reduction. The CV graph signifies that, reduction peak (R1) shows the reduction of *p*-NP to *p*-hydroxyl-amino-phenol Fig. 8(A) and the redox peaks (R2 and O1) show the oxidation of *p*-hydroxyl-amino-phenol to *p*-nitroso-phenol and the subsequent reversible reduction. Subsequently, the **MGCE** was also studied at different scan rates in the presence of *p*-NP as shown in Fig. 9. Fig. 9, shows the values of current peaks for the oxidation and reduction, increases linearly with increasing the scan rates and a linear relation was observed and plotted against the square roots of the scan rates shown in inset of Fig. 9. A higher peak potential difference (ΔEp) was found than the expected values which suggested it a highly reversible reaction. This phenomenon suggest that the electrochemical reactions taking place at the surface of GCE is quasi-reversible reaction while no significant change was found in the peak potential difference with respect to the scan rates. These observational studies clearly showing that the reactions of *p*-NP over the **MGCE** are a controlled diffusion process.

The limit of detection (LOD), was calculated using the equation, LOD = 3.3(σ/S) [37,38]. where σ is standard error and S is the slope of calibration curve and sensitivity was calculated using equation,

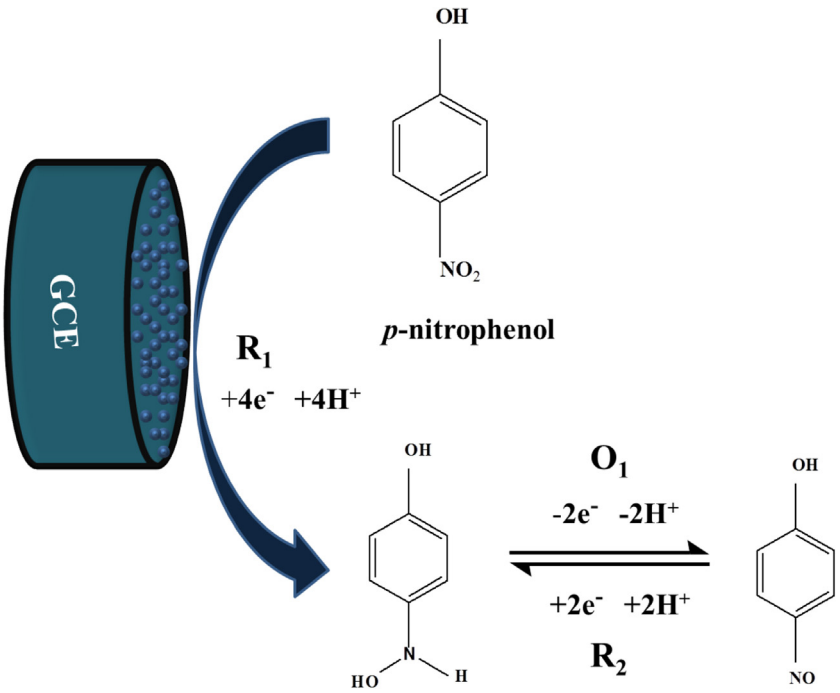

Scheme 2. Schematic representation of rGO/$SrTiO_3$ modified GCE electrode showing the reduction of *p*-nitrophenol.

Sensitivity = Slope/Area of the electrode and results are summarized in Table 1.

3.5. Comparison with the previously reported literature

There are various reports on electrochemical sensing of nitroaromatics using different modifiers for GCE and presented in Table 1 [27–31,39–49]. The reported sensors shown in Table 1 were compared with our work (**MGCE**) in terms of LOD, sensitivity and modifier used. The performance of the sensor depends on many factors such pH, type of modifier used, binder and other experimental conditions. Previous reports suggested that the electrochemical sensors have some limitations either in limit of detection or sensitivity or materials used. From Table 1 (see entry no. 1-12), it is clear that some of the reported sensors for *p*-NP (α-MnO_2 nanotube/GCE, Mg(Ni)FeO/CPE, ZnO/GCE, Nanogold/GCE, Poly(propyleneimine)–gold/GCE, MWCNT/GCE and Silver particles/GCE) have not shown considerable good limit of detection as compare to our present work (**MGCE**). While in other cases (Ordered mesoporous carbon/GCE, CuO nanotube/GCE, MWNT-Nafion/GCE and Nano-Cu_2O/Pt electrode) the limit of detection is comparable or less sensitivity (in few case sensitivity data not shown) for the reported sensors compare to our results. For other studied nitroaromatics, the results are quite interesting and calculated LOD and sensitivity for the MGCE is considerably good compare to previous reports (see entry no. 13–18). Our constructed **MGCE** shows better performance in terms of studied parameters (LOD, sensitivity, stability, reproducibility and repeatability) for

Table 1
Summary of the LOD, Sensitivity and Linear range of the nitroaromatics with previously reported literature.

No.	Electrode	Nitro-aromatics	Limit of detection (LOD) (nM)	Sensitivity	Linear range (μM)	References
1.	α-MnO_2 nanotube/GCE	*p*-NP	100000	19.18 mA/mMcm^2	100–700	39
2.	Ordered mesoporous carbon/GCE	*p*-NP	100	–	2–90	40
3.	Mg(Ni)FeO/CPE	*p*-NP	200	0.811 mA/mMcm^2	2–200	41
4.	CuO nanotube/GCE	*p*-NP	5	0.132 mA/mMcm^2	0.01–1000	42
5.	ZnO/GCE	*p*-NP	13000	404.35 μA/mMcm^2	0.01–1000	43
6.	MWNT-Nafion/GCE	*p*-NP	40	–	0.1–1	44
7.	Nanogold/GCE	*p*-NP	8000	–	10–1000	45
8.	Poly(propyleneimine)–gold/GCE	*p*-NP	450	–	0.61–625	46
9.	MWCNT/GCE	*p*-NP	400	–	2–4000	47
10.	Nano-Cu_2O/Pt electrode	*p*-NP	100	–	10–1000	48
11.	Silver particles/GCE	*p*-NP	500	–	1.5–140	49
12.	MGCE	*p*-NP	110	193.4 μA/μMcm^2	0.3–0.8	*This Work*
13.	Screen printed electrode	2,4-DNT	700	–	1–200	27
14.	Electrochemically Reduced Graphene	2,4-DNT	42	–	–	28
15.	N-rGO/CuS	TNP	69	–	–	29
16.	Functionalized reduced graphene oxide	TNP	540	0.00613 μA/μM	5–215	30
17.	Sonogel carbon	TNP	2800	–	–	31
18.	MGCE	2,4-DNP	134	25.34 μA/μMcm^2	0.4–0.7	
	MGCE	2,4-DNT	128	71.66 μA/μMcm^2	0.5–0.8	*This Work*
	MGCE	TNP	146	13.16 μA/μMcm^2	0.5–0.7	

Table 2
Nitroaromatics recovery analysis for real water sample.

Sample (Tape Water)	Added(μM) [a]	Found (μM)[b]	Recovery (%)[b]	RSD (%)[b]
p-NP	0	0	0	0
	0.5	0.47	94	2.5
	1	0.97	97	1.71
2,4-DNP	0	0	0	0
	0.5	0.52	105.8	3.2
	1	1.01	101	1.90
2,4-DNT	0	0	0	0
	0.5	0.49	98	2.84
	1	1.03	103.3	1.68
TNP	0	0	0	0
	0.5	0.48	96	02.15
	1	1.01	101.2	1.26

[a] Average value of three measurements.
[b] Average value for proposed method.

the detection of all four nitroaromatics and the obtained results are considerable good compare to previously reported sensors.

3.6. Reproducibility, repeatability and stability

The reproducibility of the **MGCE** was evaluated by performing cyclic voltammetry in presence of 0.5 μM *p*-NP for 8 times using the same electrode and no significant variation was observed in terms of over potential and current response which suggested that the response of **MGCE** against measured species can be easily reproduced. To check the repeatability of **MGCE**, the two **MGCE** electrodes were prepared and their current response towards 0.5 μM *p*-NP in PBS (pH 7.0) was tested with a scan potential of 100 mV/s, negligible variation in current response was observed which revealed that **MGCE** electrodes can be repeated with a relative standard deviation of 2.94%. Further, the stability of the **MGCE** was checked for 12 days and no significant change in current response with a relative standard deviation of 3.12% was obtained which confirmed the stability of the **MGCE**.

3.7. Interference study

For a strong effective sensor of any material, the sensor should have anti-interfering properties. To evaluate the selectivity, a competitive effect of interference species on the electrochemical behavior of the **MGCE** sensor was studied using DPV and chronoamperometry. Fig. 13A shows the DPVs of the **MGCE** in presence of 0.1 μM *p*-NP (Fig. 13A (a)) and 1 μM (Fig. 13A (k)) in presence of other interference species such as phenol, toluene, chlorophenol, catechol, chlorobenzene, Na^+, Mg^{2+}, K^+ and Cl^- (Fig. 13A (b–j)). The addition of interference species have the negligible current response without change in the over potential of the *p*-NP (Fig. 13A, (a–k)). The concentration of the interference species (5 μM) was 50 times higher than *p*-NP (0.1 μM). A very high current response was obtained by the addition of 0.5 μM *p*-NP compare to other interfering species. These results revealed that interference species does not alter the performance of the developed **MGCE** sensor and is highly selective towards *p*-NP. Further, chronoamperometry was employed to check the selectivity of four nitroaromatics (*p*-NP, 2,4-DNP, 2,4-DNT and TNP). Fig. 13B shows the effect of interference species, it was observed that with addition of *p*-NP, 2,4-DNP, 2,4-DNT and TNP current increases rapidly whereas on the addition of interference species (toluene, phenol, chlorophenol, catechol, chlorobenzene, Na^+, Mg^{2+}, K^+ and Cl^-) no considerable change in current response was observed. Hence, both the techniques confirm that **MGCE** is highly selective towards nitroaromatics.

3.8. Real sample analysis

Real sample analysis for the **MGCE** sensor was performed using standard addition method. The obtained results were summarized in Table 2. To check the performance of developed sensor, the real sample analysis was evaluated on tap water. The cyclic voltammetry (CV) of real sample was carried out using the tape water as a control and results show that absence of any measured nitroaromatic. Further, the tape water sample was spiked with 0.5 μM and 1 μM of *p*-NP, 2,4DNP, 2,4-DNT and TNP. The prepared samples were analyzed by using CV and different analytical parameters have been calculated which are listed in Table 2.

4. Conclusion

In summary, we reported the facile *insitu* synthesis of rGO/$SrTiO_3$ nanocomposite.The binder free modified electrode (**MGCE**) was fabricated using rGO/$SrTiO_3$ composite on the GCE by simple drop cast method. The **MGCE** was further monitored and showed the excellent electro-catalytic response against different nitroaromatics. The binder free **MGCE** exhibited the limit of detection (LOD) 110 nM, 134 nM, 128 nM, 146 nM and a high sensitivity 193.43 μA $\mu M^{-1} cm^{-2}$, 25.34 μA $\mu M^{-1} cm^{-2}$, 71.66 μA $\mu M^{-1} cm^{-2}$, 13.16 μA $\mu M^{-1} cm^{-2}$ for *p*-NP, 2,4-DNP, 2,4-DNT and TNP, respectively, which reveal that **MGCE** exhibited a better response for *p*-NP among other nitroaromatics. The plausible mechanism for electrochemical detection of *p*-NP has been discussed. **MGCE** can be further used in the fabrication of binder free explosive sensors. To the best of our knowledge, this is the first report to detect four nitroaromatics with single modified electrode.

Acknowledgements

SMM would like to acknowledge CSIR, New Delhi and IIT Indore for funding and Sophisticated Instrumentation Centre (SIC), IIT Indore for providing the characterization facility. We also thank the Advanced Imaging Center, IIT Kanpur for providing TEM facility. KA and AM would like to thank to UGC, New Delhi for providing research fellowship (RGNF-D) No. F./201415/RGNF201415DOBCUTT57599 and MHRD, Govt. of India, New Delhi, India, respectively. PM gratefully acknowledges J. C. Bose National Fellowship.

Appendix A. Supplementary data

Supplementary data associated with this article can be found, in the online version, at http://dx.doi.org/10.1016/j.electacta.2016.08.123.

References

[1] N.C. Bristowe, J. Varignon, D. Fontaine, E. Bousquet, Ph. Ghosez, Ferromagnetism induced by entangled charge and orbital orderings in ferroelectric titanate perovskites, Nat. Commun. 6 (2015) 1–8.
[2] A. Bera, K. Wu, A. Shaikh, E. Alarousu, O.F. Mohammed, T. Wu, Perovskite Oxide $SrTiO_3$ as an Efficient Electron Transporter for Hybrid Perovskite Solar Cells, J. Phys. Chem. C 118 (2014) 28494–28501.
[3] S. Tonda, S. Kumar, O. Anjaneyulu, V. Shanke, Synthesis of Cr and La-codoped $SrTiO_3$ nanoparticles for enhanced photocatalytic performance under sunlight irradiation, Phys. Chem. Chem. Phys. 16 (2014) 23819–23828.
[4] Z. Shen, Z. Wang, B. Luo, L. Li, $BaTiO_3$–$BiYbO_3$ perovskite materials for energy storage applications, J. Mater. Chem. A 3 (2015) 18146–18153.
[5] D.K. Hwang, S. Kim, J.H. Lee, I.S. Hwang, I.I.-D. Kim, Phase evolution of perovskite $LaNiO_3$ nanofibers for supercapacitor application and p-type gas

sensing properties of LaOCl–NiO composite nanofibers, J. Mater. Chem. 21 (2011) 1959–1965.
[6] G. Dong, H. Fan, T. Tian, J. Fang, Q. Li, Gas-sensing and electrical properties of perovskite structure p-type barium-substituted bismuth ferrite, RSC Adv. 5 (2015) 29618–29623.
[7] J.W. Fergus, Perovskite oxides for semiconductor-based gas sensors, Sens. Actuators B Chem. 123 (2007) 1169–1179.
[8] S. Singh, A. Singh, B.C. Yadav, P.K. Dwivedi, Fabrication of nanobeads structured perovskite type neodymium iron oxide film: its structural, optical, electrical and LPG sensing investigations, Sens. Actuators B Chem. 177 (2013) 730–739.
[9] B. Wang, B. Gu, Y. Ding, Y. Chu, Z. Zhang, B. Ba, Q. Zhang, X. Li, A novel route to prepare LaNiO3 perovskite-type oxide nanofibers by electrospinning for glucose and hydrogen peroxide sensing, Analyst 138 (2013) 362–367.
[10] D. Chen, H. Zhang, Y. Liu, J. Li, Graphene and its derivatives for the development of solar cells photoelectrochemical, and photocatalytic applications, Energy Environ. Sci. 6 (2013) 1362–1387.
[11] N. Gao, X. Fang, Synthesis and Development of Graphene–Inorganic Semiconductor Nanocomposites, Chem. Rev. 115 (2015) 8294–8343.
[12] C. Zhao, S.L. Chou, Y. Wang, C. Zhou, H.K. Liu, S.X. Dou, A facile route to synthesize transition metal oxide/reduced graphene oxide composites and their lithium storage performance, RSC Adv. 3 (2013) 16597–16603.
[13] H.K. Kim, S.H. Park, S.B. Yoon, S.B.C.W. Lee, J.H. Jeong, K.C. Roh, K.B. Kim, In Situ Synthesis of Three-Dimensional Self-Assembled Metal Oxide–Reduced Graphene Oxide Architecture, Chem. Mater. 26 (2014) 4838–4843.
[14] J. Wang, Electrochemical Sensing of Explosives, Electroanalysis 19 (2007) 415–423.
[15] J.A. Padilla-Sa'nchez, P. Plaza-Bolaños, R. Romero-Gonza'lez, A. Garrido-Frenich, J.L.M. Vidal, Application of a quick, easy, cheap, effective, rugged and safe-based method for the simultaneous extraction of chlorophenols, alkylphenols, nitrophenols and cresols in agricultural soils, analyzed by using gas chromatography-triple quadrupole-mass spectrometry/mass spectrometry, J. Chromatogr. A 1217 (2010) 5724–5731.
[16] S.P. Wang, H.J. Chen, Separation and determination of nitrobenzenes by micellar electrokinetic chromatography and high-performance liquid chromatography, J. Chromatogr. A 979 (2002) 439–446.
[17] W. Zhang, C.R. Wilson, N.D. Danielson, Indirect fluorescent determination of selected nitro-aromatic and pharmaceutical compounds via UV-photolysis of 2-phenylbenzimidazole-5-sulfonate, Talanta 74 (2008) 1400–1407.
[18] X. Guo, Z. Wang, S. Zhou, The separation and determination of nitrophenol isomers by high-performance capillary zone electrophoresis, Talanta 64 (2004) 135–139.
[19] Y. Tang, R. Huang, C. Liu, S. Yang, Z. Lu, S. Luo, Electrochemical detection of 4-nitrophenol based on a glassy carbon electrode modified with a reduced graphene oxide/Au nanoparticle composite, Anal. Methods 5 (2013) 5508–5514.
[20] A.M. O'Mahony, J. Wang, Nanomaterial-based electrochemical detection of explosives: a review of recent developments, Anal. Methods 5 (2013) 4296–4309.
[21] J.S. Caygill, F. Davis, S.P.J. higson, Current trends in explosive detection techniques Higson, Talanta 88 (2012) 14–29.
[22] M. Abaker, G.N. Dar, A. Umar, S.A. Zaidi, A.A. Ibrahim, S. Baskoutas, A. Hajry, CuO Nanocubes Based Highly-Sensitive 4-Nitrophenol Chemical Sensor, Sci. Adv. Mater. 4 (2012) 893–900.
[23] J. Wu, Q. Wang, A. Umar, S. Sun, L. Huang, J. Wang, J. Gao, Highly sensitive p-nitrophenol chemical sensor based on crystalline α-MnO_2 nanotubes, New J. Chem. 38 (2014) 4420–4426.
[24] A. Sinhamahapatra, D. Bhattacharjya, J.S. Yu, Green fabrication of 3-dimensional flower-shaped zinc glycerolate and ZnO microstructures for p-nitrophenol sensing, RSC Adv. 5 (2015) 37721–37728.
[25] Y. Tang, R. Huang, C. Liu, S. Yang, Z. Lu, S. Luo, Electrochemical detection of 4-nitrophenol based on a glassy carbon electrode modified with a reduced graphene oxide/Au nanoparticle composite, Anal. Methods 5 (2013) 5508–5514.
[26] Y. Xu, Y. Wang, Y. Ding, L. Luo, X. Liu, Y. Zhang, Determination of p-nitrophenol on carbon paste electrode modified with a nanoscaled compound oxide Mg (Ni)FeO, J. Appl. Electrochem. 43 (2013) 679–687.
[27] J.S. Caygill, S.D. Collyer, J.L. Holmes, F. Davisa, S.P.J. Higson, Disposable screen-printed sensors for the electrochemical detection of TNT and DNT, Analyst 138 (2013) 346–352.
[28] T.W. Chen, Z.H. Sheng, K. Wang, F.B. Wang, X.H. Xia, Determination of Explosives Using Electrochemically Reduced Graphene, Chem. Asian J. 6 (2011) 1210–1216.
[29] K. Giribabu, S.Y. Oh, R. Suresh, S.P. Kumar, R. Manigandan, S. Munusamy, G. Gnanamoorthy, J.Y. Kim, Y.S. Huh, V. Narayanan, Sensing of picric acid with a glassy carbon electrode modified with CuS nanoparticles deposited on nitrogen-doped reduced graphene oxide, Microchim Acta 183 (2016) 2421–2430.
[30] J. Huang, L. Wang, C. Shi, Y. Dai, C. Gu, J. Liu, Selective detection of picric acid using functionalized reduced graphene oxide sensor device, Sens and Actuators B Chem. 196 (2014) 567–573.
[31] R.M. del Mar, I.N. Rodríguez, J.M. Palacios-Santander, L.M. Cubillana-Aguilera, J. L. Hidalgo-Hidalgo-de-Cisneros, Study of the Responses of a Sonogel-Carbon Electrode Towards Phenolic Compounds, Electroanal. 17 (2005) 806–814.
[32] J.S. Caygill, F. Davis, S.P.J. Higson, Current trends in explosive detection techniques, Talanta 88 (2012) 14–29.
[33] D.C. Marcano, D.V. Kosynkin, J.M. Berlin, A. Sinitskii, Z. Sun, A. Slesarev, L.B. Alemany, W. Lu, J.M. Tour, Improved Synthesis of Graphene Oxide, ACS Nano 4 (2010) 4806–4814.
[34] C.S.R. Vusa, S. Berchmans, S. Alwarappan, Facile and green synthesis of graphene, RSC Adv. 4 (2014) 22470–22475.
[35] S. Ouyang, H. Tong, N. Umezawa, J. Cao, P. Li, Y. Bi, Y. Zhang, J. Ye, Surface-Alkalinization-Induced Enhancement of Photocatalytic H_2 Evolution over $SrTiO_3$-Based Photocatalysts, J. Am. Chem. Soc. 134 (2012) 1974–1977.
[36] J. Zhang, J.H. Bang, C. Tang, P.V. Kamat, Tailored TiO_2-$SrTiO_3$ Heterostructure Nanotube Arrays for Improved Photoelectrochemical Performance, ACS Nano 4 (2010) 387–395.
[37] A.K. Saini, M. Srivastava, V. Sharma, V. Mishra, S.M. Mobin, A highly selective, sensitive and reversible fluorescence chemosensor for Zn^{2+} and its cell viability, Dalton Trans. 45 (2016) 3927–3935.
[38] K. Ahmad, A. Mohammad, R. Rajak, S.M. Mobin, Construction of TiO_2 nanosheets modified glassy carbon electrode (GCE/TiO_2) for the detection of hydrazine, Mater. Res. Express 3 (2016) 074005.
[39] J. Wu, Q. Wang, A. Umar, S. Sun, L. Huang, J. Wanga, Y. Gao, Highly sensitive *p*-nitrophenol chemical sensor based on crystalline α-MnO_2 nanotubes, New J. Chem. 38 (2014) 4420–4426.
[40] R.C. Reid, J.M. Prausnitz, B.E. Poling, The properties of gases and liquids, McGraw-Hill, New York, 1987.
[41] Y. Xu, Y. Wang, Y. Ding, L. Luo, X. Liu, Y. Zhang, Determination of *p*-nitrophenol on carbon paste electrode modified with a nanoscaled compound oxide Mg (Ni)FeO, J. Appl. Electrochem. 43 (2013) 679–687.
[42] M. Abaker, G.N. Dar, A. Umar, S.A. Zaidi, A.A. Ibrahim, S. Baskoutas, A. Al-Hajry, CuO Nanocubes Based Highly-Sensitive 4-Nitrophenol Chemical Sensor, Sci. Adv. Mater. 4 (2012) 893–900.
[43] A. Sinhamahapatra, D. Bhattacharjya, J. Yu, Green fabrication of 3-dimensional flower-shaped zinc glycerolate and ZnO microstructures for *p*-nitrophenol sensing, RSC Adv. 5 (2015) 37721–37728.
[44] W. Huang, C. Yang, S. Zhang, Simultaneous determination of 2-nitrophenol and 4-nitrophenol based on the multi-wall carbon nanotubes Nafion-modified electrode, Anal. Bioanal. Chem. 375 (2003) 703–707.
[45] L. Chu, L. Han, X. Zhang, Electrochemical simultaneous determination of nitrophenol isomers at nano-gold modified glassy carbon electrode, J. Appl. Electrochem. 41 (2011) 687–694.
[46] T. Ndlovu, O.A. Arotiba, R.W. Krause, B.B. Mamba, Electrochemical Detection of o-Nitrophenol on a Poly(propyleneimine)-gold Nanocomposite Modified Glassy Carbon Electrode, Int. J. Electrochem. Sci. 5 (2010) 1179–1186.
[47] C. Yang, Electrochemical Determination of 4-Nitrophenol Using a Single-Wall Carbon Nanotube Film-Coated Glassy Carbon Electrode, Microchim. Acta 148 (2004) 87–92.
[48] Y. Gu, Y. Zhang, F. Zhang, J. Wei, C. Wang, Y. Du, W. Ye, Investigation of photoelectrocatalytic activity of Cu2O nanoparticles for p-nitrophenol using rotating ring-disk electrode and application for electrocatalytic determination, Electrochim. Acta 56 (2010) 953–958.
[49] I.G. Casella, M. Contursi, The Electrochemical Reduction of Nitrophenols on Silver Globular Particles Electrodeposited under Pulsed Potential Conditions, J. Electrochem. Soc. 154 (2007) 697–702.